

Article

Reduced Graphene Oxide Supported Cobalt-Calcium Phosphate Composite for Electrochemical Water Oxidation

Keunyoung Lee¹, Wonseok Yang², Eunji Pyo¹, Hyebin Choi¹, Yeona Cha¹, Seonhong Lee³ , Chung Soo Kim³, Dong-Kwon Lim^{2,*} and Ki-Young Kwon^{1,*}

¹ Department of Chemistry, Gyeongsang National University, Jinju 52828, Korea; sofiato96@gnu.ac.kr (K.L.); eunji2684@gnu.ac.kr (E.P.); gpqls3214@gnu.ac.kr (H.C.); yooona20@gnu.ac.kr (Y.C.)

² KU-KIST Graduate School of Converging Science and Technology, Korea University, Seoul 02841, Korea; wowbluesky@korea.ac.kr

³ Analysis & Certification Center, Korea Institute of Ceramic Engineering & Technology, Jinju 52851, Korea; sh0381@kicet.re.kr (S.L.); cskim@kicet.re.kr (C.S.K.)

* Correspondence: dklim@korea.ac.kr (D.-K.L.); kykwon@gnu.ac.kr (K.-Y.K.); Tel.: +82-2-3290-4611 (D.-K.L.); +82-55-772-1493 (K.-Y.K.)

Abstract: We report the oxygen evolution reaction (OER) catalyst composed of cobalt–calcium phosphate on reduced graphene oxide (CoCaP/rGO). Our catalyst is prepared by the anodic electrolysis of calcium phosphate/rGO mixture loaded on indium-tin-oxide (ITO) in Co²⁺ aqueous solution. TEM, XPS and XRD experiments confirm that the crystal phase of calcium phosphate (CaP) is transferred into an amorphous phase of calcium oxide with phosphate (5.06 at%) after anodic electrolysis. Additionally, the main cation component of calcium is replaced by cobalt ion. The current–voltage characteristics of CoCaP/rGO showed a shoulder peak at 1.10 V vs. NHE, which originated from Co²⁺ to higher oxidation states (Co³⁺ or Co⁴⁺) and a strong wave from water oxidation higher +1.16 V vs. NHE at neutral condition (pH 7). CoCaP and CoCaP/rGO showed 4.8 and 10 mA/cm² at 0.47 V of overpotential, respectively. The enhanced OER catalytic activity of CoCaP/rGO arises from the synergetic interaction between the amorphous phase of CoCaP and electric conducting graphene sheets.

Keywords: OER; calcium phosphate; graphene



Citation: Lee, K.; Yang, W.; Pyo, E.; Choi, H.; Cha, Y.; Lee, S.; Kim, C.S.; Lim, D.-K.; Kwon, K.-Y. Reduced Graphene Oxide Supported Cobalt-Calcium Phosphate Composite for Electrochemical Water Oxidation. *Catalysts* **2021**, *11*, 960. <https://doi.org/10.3390/catal11080960>

Academic Editor: Enric Brillas

Received: 14 July 2021

Accepted: 10 August 2021

Published: 11 August 2021

Publisher's Note: MDPI stays neutral with regard to jurisdictional claims in published maps and institutional affiliations.



Copyright: © 2021 by the authors. Licensee MDPI, Basel, Switzerland. This article is an open access article distributed under the terms and conditions of the Creative Commons Attribution (CC BY) license (<https://creativecommons.org/licenses/by/4.0/>).

1. Introduction

As the demand for sustainable energy increases, much research has been conducted on the development of renewable and environmentally benign energy [1]. In regard to solar energy conversion into chemical energy, water splitting has been extensively investigated for last three decades. Especially, electrochemical catalysts that enable the water oxidation have been considered as critical factor to improving the energy conversion efficiency. So far, precious metals or precious metals oxides (e.g., Ru/Ir oxides) are regarded as the prototype of oxygen evolution reaction (OER) catalysts [2–6]. However, these precious metals cannot be generally used because of their high cost [7,8]. Therefore, it is necessary to develop alternative catalysts that are made of relatively low-cost and earth-abundant elements with catalytic activity and durability. Hence, comparatively inexpensive transition metals (cobalt [9–11], copper [12], iron [13,14], etc.) deposited on carbon-based substrates graphene [15–17] and carbon nanotubes [18–20]) have been widely investigated. Generally, transition metal oxide/phosphates have insufficient electrical conductivity and a low surface area, which result in sluggish kinetics during the OER. Meanwhile, graphene oxide (GO) based materials have been widely used for oxygen/hydrogen evolution reaction and oxygen reduction reaction (ORR) because of their atomic thinness and high electrical conductivity after the reduction treatment [21–24]. For example, Co₃O₄ nanoparticles reduced graphene oxide (rGO) [25], cobalt oxide on crumpled graphene with a high surface

area [26], iron and nickel on GO [27], solvothermal synthesis of NiCo_2S_4 nanoparticles on rGO [28] and GO-incorporated Cu-MOF composite [29] were utilized for HER, OER and ORR catalysts. The Nocera group demonstrated that an amorphous cobalt oxide containing phosphate group (so called Co-Pi) exhibited excellent OER catalytic properties under neutral pH conditions [30–36]. This Co-Pi has been successfully prepared on various substrates by in situ anodic electrolysis in phosphate buffer containing a small number of cobalt ions [31,37]. Previously, we developed a noble preparation method for the cobalt phosphate catalyst [38]. Particularly, we utilized the solid phase of hydroxyapatite (HAP) as a phosphate source instead of a solution phase of phosphate buffer. Our catalysts were prepared by the ion-exchange reaction of HAP (CoHAP) with aqueous cobalt ions solution [39]. Here, we developed the CoCaP/rGO OER catalyst through the anodic electrolysis of calcium phosphate and graphene mixture loaded on ITO under aqueous Co^{2+} solution. After the anodic electrolysis, the calcium phosphate crystallites are changed into an amorphous cobalt oxide/phosphate. In addition, these cobalt oxide/phosphates are well dispersed in rGO without aggregation. Therefore, CoCaP/rGO exhibits enhanced OER catalytic activity compared to CoCaP (CoCaP/rGO requires only 457 mV to drive 10 mA). Furthermore, the Tafel slope was improved after the incorporation of Co^{2+} ions (239 mV/dec to 132 mV/dec).

2. Results

CoCaP/rGO is synthesized in two steps. First, CaP/rGO is prepared by the precipitation from the mixture of aqueous solution containing rGO, Ca^{2+} and HPO_4^- . The ink of CaP/rGO is loaded onto the ITO substrate. Second, CaP/rGO is electrochemically converted into CoCaP/rGO by anodic electrolysis in the Co^{2+} aqueous solution.

Figure 1a shows the grayish color of CaP/rGO on ITO. Calcium phosphate and rGO are white and black colored, respectively. The mixture loaded on an ITO exhibits a gray color. After the anodic electrolysis of CaP/rGO in the Co^{2+} aqueous solution for 60 min, the gray color of CaP/rGO is changed into a dark brown (Figure 1b, Supplementary Video S1). The dark brown color was previously reported in the OER catalyst based on Co-Pi [40–42]. Figure 1c represents the current density profile during anodic electrolysis. The current density is the highest at 5 min and gradually decreases, then reaches the baseline level after 20 min. These currents seem to be caused by the charge transfer involved in the CoCaP/rGO formation, not by the faradaic current of water oxidation. CoCaP/rGO is precipitated on ITO by the reaction between the phosphate group of calcium phosphate and the Co^{2+} in aqueous solution, in which Co^{2+} is changed into $\text{Co}^{3+}/\text{Co}^{4+}$ given bias (+1.3 V vs. NHE). The total charge flow for 60 min is 150 mC/cm². For the control experiment, the current density profile of the bare ITO electrode without CaP/rGO is carried out under the same electrolysis condition (Figure 1c). In this case, the current is barely flowed and the color of the ITO is light yellow (Supplementary Figure S1), which is obviously different from the dark brown color of CoCaP/rGO film. Figure 1d shows the change of XRD patterns before and after anodic electrolysis. The calcium phosphate from the reaction of calcium nitrate and sodium phosphate dibasic is well matched with monetite (CaHPO_4 , JCPDS No. 70-1425, marked with red dots) patterns. The average crystal size of CaP is 33.9 nm based on a calculation by the Scherrer equation (Supplementary Figure S2). After anodic electrolysis, the diffraction patterns of the monetite disappeared. In addition, no new diffraction patterns are observed. Therefore, we interpret that the monetite crystallite is changed into an amorphous form of cobalt/oxides in which the amorphous morphology of cobalt phosphate improves OER activity in the previous report [43,44].

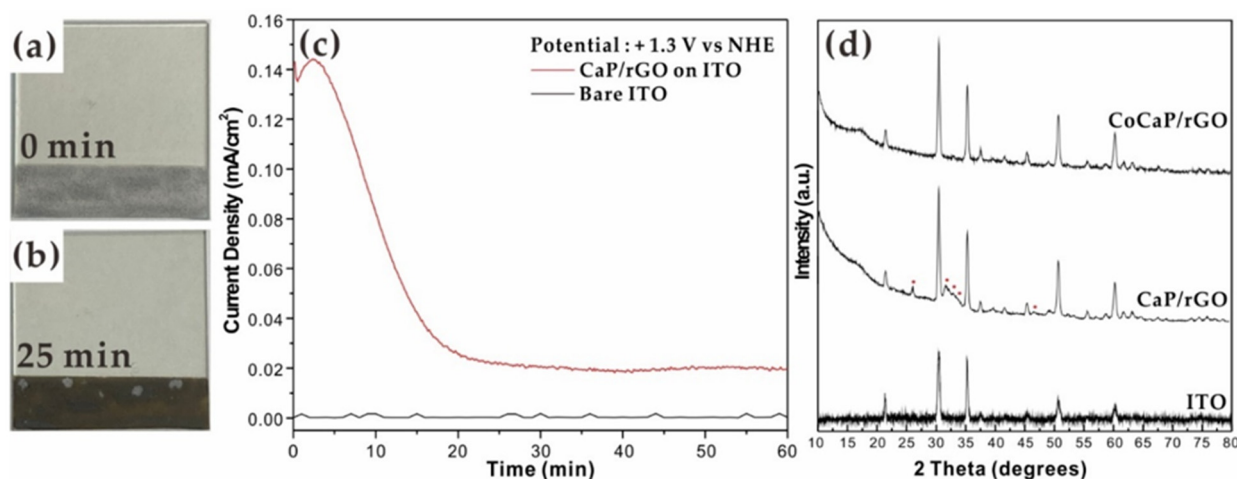


Figure 1. Photographs of (a) CaP/rGO and (b) CoCaP/rGO film on ITO after anodic electrolysis for 25 min. (c) Current density for anodic electrolysis at +1.3 V vs. NHE in 20 mM Co²⁺. (d) XRD patterns of CaP/rGO, CoCaP/rGO loaded on ITO electrode, CaHPO₄ (monetite) and ITO electrode.

TEM and EDS elemental mappings are performed to investigate the morphology and local/surface elemental distribution of CaP/rGO and CoCaP/rGO. CaP/rGO (Supplementary Figure S3) shows elongated shape of about 40.1 nm in width and 97.3 nm in length, on average. Previously, we investigated the impact of pH on the morphology of calcium phosphate in which monetite with an elongated shape is formed when the base is not added, as in this study [45]. CoCaP/rGO composite (Figure 2a,b), on the other hand, does not exhibit a distinct shape. These features are similarly observed in SEM images (Supplementary Figure S3). Therefore, we concluded that the anodic electrolysis is accompanied by the absence of diffraction patterns of monetite and morphology changes (Figure 1d, Figure 2 and Supplementary Figure S2). In addition, TEM-EDS mapping measurements (Figure 2c–i) show that all chemical species, especially cobalt ions, are evenly distributed in the entire sample of CoCaP/rGO without local aggregation. TEM-EDS analysis indicates that after the anodic electrolysis in the Co²⁺ aqueous solution, the atomical composition of Ca²⁺ decreased from 12.24 at% to 0.48 at%. Meanwhile, those of Co²⁺ increased by 3.61 at%. The main cation of calcium ion is replaced by the cobalt ion after the anodic electrolysis. According to SEM images, the elongated crystallites of CaP/rGO cannot be distinguishable after the anodic electrolysis for an hour. The SEM-EDS elemental mapping measurements showed consistent results with the TEM-EDS experiments. The surface composition of the samples is analyzed by an X-ray photoelectron spectrum (XPS). The survey spectrum (Figure 3a) of the CaP/rGO and CoCaP/rGO confirms the presence of the carbon, calcium, oxygen, phosphorous and cobalt. While the Ca 2s and 2p peak of CaP/rGO almost disappeared after the anodic electrolysis, an additional new peak of Co 2p is observable. Based on the quantitative analysis by XPS, the atomic percentage of calcium is estimated as 6.54% for the CaP/rGO composite. After the anodic electrolysis, the atomic percentages of calcium decreased by 0.05%, while the cobalt species was 1.8%. The trend change of the elemental change is consistent with TEM-EDS (Figure 2c–2i). Therefore, we confirm that the main cation of composite changed from calcium to cobalt after the anodic electrolysis. High resolution Co 2p XPS spectra show 2p_{3/2} and 2p_{1/2} peaks for cobalt at 780.95 and 795.18 eV [46]. Co species is considered to be mainly in the 2+ oxidation state. Additionally, the Co 2p_{3/2} with a shoulder peak indicates that CoCaP/rGO may contain cobalt cations in the form of both Co²⁺ and Co³⁺ cations [37,47]. Supplementary Figure S4 represents that a phosphorous 2p peak at 132.78 eV indicates the existence of phosphate in CoCaP/rGO [48,49].

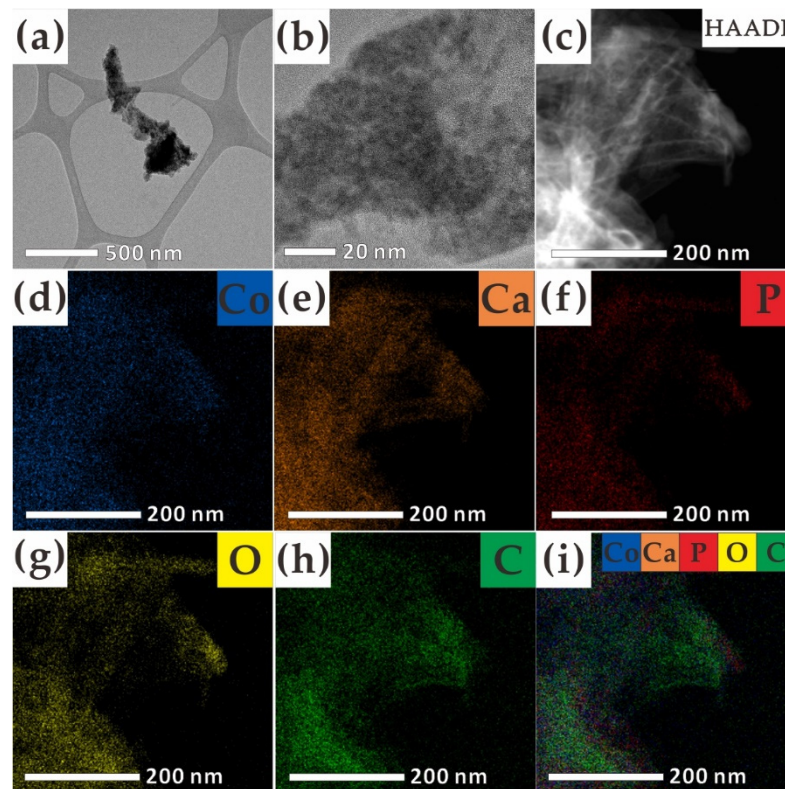


Figure 2. TEM images of (a) CoCaP/rGO, (b) a high resolution TEM image of CoCaP/rGO and EDS elements mapping of CoCaP/rGO, (c) a TEM image, (d) Co, (e) Ca, (f) P, (g) O, (h) C and (i) an overlapping of Co, Ca, P, O, C.

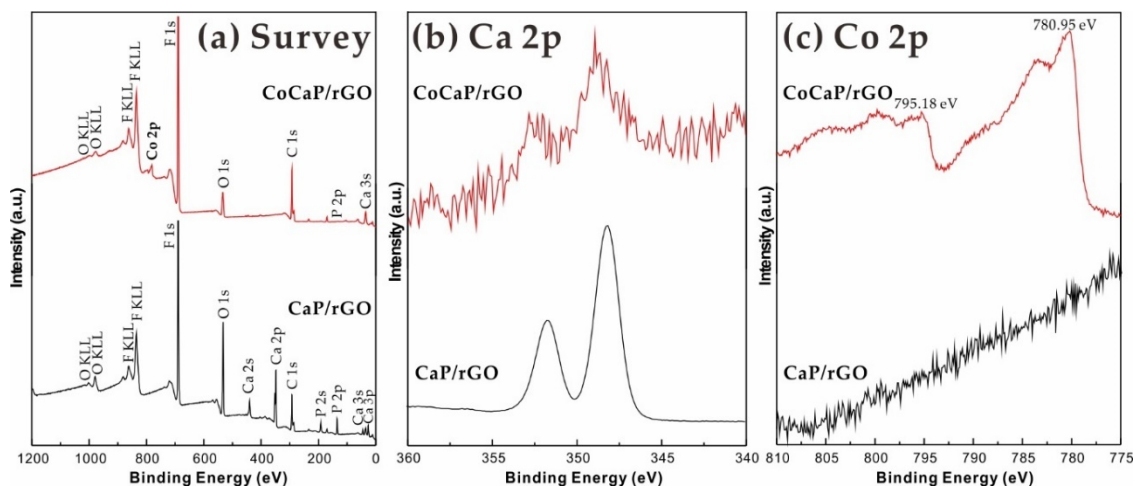


Figure 3. XPS spectrum of (a) Survey, (b) Ca 2p and (c) Co 2p of CaP/rGO and CoCaP/rGO. (Fluorine signal originated from Nafion.)

The electrochemical characterizations (cyclic voltammetry (CV), linear sweep voltammetry (LSV) and bulk electrolysis) of CoCaP and CoCaP/rGO are performed by commercial potentiostat with three electrode system under neutral pH conditions (0.1 M KPi, pH 7). Details are described in the experimental method. Figure 4a shows the cyclic voltammetry of CaP and CoCaP/rGO on a glassy carbon electrode (5 mm diameter). The oxidative wave at +1.1 V vs. NHE is observed from both the CV and LSV curves of CoCaP/rGO (Figure 4a,b). This shoulder is commonly observed in Co-Pi catalysts and originated from the $\text{Co}^{2+}/\text{Co}^{3+}$ or Co^{4+} transitions [33,35,37,50–52]. Figure 4b presents LSV curves with a sweep rate of 5 mV/s in 0.1 M KPi (pH 7). The current densities of CoCaP and CoCaP/rGO

exhibit 3.5 mA/cm^2 and 15 mA/cm^2 at 1.3 V vs. NHE, respectively. Due to their low electric conductivity, transition metal oxide/phosphates combined with rGO and CoCaP significantly induces the improvement of OER catalytic activity. The improvements of ORR and HER catalytic activity are additionally reported by the hybrid of the catalyst and GO [53–55]. Previously, we reported that cobalt incorporated hydroxyapatite (CoHAP) OER catalyst. CoCaP/rGO showed approximately ten-fold higher OER activity than CoHAP (1.2 mA/cm^2 at 1.3 V vs. NHE). CoHAP is prepared by the ion exchange reaction of HAP by the simple immersion of HAP in aqueous Co^{2+} solution, in which cobalt ions are coated on the surface of HAP. Therefore, the number of cobalt species in CoHAP is much less than that of cobalt species in CoCaP/rGO prepared by anodic electrolysis. The electrochemical active surface area of both samples is determined by measuring double-layer capacitance using CV at different scan rates (20, 30, 50, 100 and 200 mV/s) in the potential region having no Faradaic current (Figure 4c and Figure S6). The capacitance of CoCaP/rGO is approximately eleven-fold over that of CoCaP. Therefore, the increased catalytic active area by the dispersion of CoCaP on rGO surface enhances OER catalytic activity. Figure 4d and Supplementary Movie S2 illustrate a stability of CoCaP and CoCaP/rGO loaded on ITO as a working electrode at the overpotential of 680 mV through the bulk electrolysis over 24 h. Both CoCaP/rGO and CoCaP present durability with 90% and 95% after the potential is applied. The electrocatalytic properties of both CaP/rGO and CoCaP/rGO composite (Figure 4e) are estimated by Tafel plots and showed linearity in the range of ca. 100 mV of overpotentials. The Tafel slope for CoCaP/rGO shows an improved activity with a slope of 132 mV/dec compared to the that of CoCaP (239 mV/dec). This lower value is comparable to other Tafel slopes of cobalt based OER catalysts performed under pH 7 conditions (166 mV/dec for Co-Bi nanoarray [56], 121 mV/dec for $\text{CoFe}(\text{CN})_5\text{-PVP}$ [57], $89\text{--}95 \text{ mV/dec}$ for Co/Fe PBAs [58] and 137 mV/dec for CoO/CoSe_2 hybrid [59] electrocatalysts). The improved OER activity and Tafel slope of CoCaP/rGO seem to originate from the efficient charge transfer from rGO to active catalytic species due to the well dispersion of CoCaP on rGO. Generally, transition metal oxide or phosphates exhibit poor electric conductivity. Therefore, combining active catalytic species with carbon supports has been widely applied in catalytic system of OER or ORR. For example, NiCo double hydroxide on N-doped graphene [60], CoFe_2O_4 on graphene [61] and graphene- Co_3O_4 nanocomposite [62] were demonstrated for OER catalysts with higher OER/ORR activities and material durability. In addition to the charge transfer issue, the dispersion of CoCaP on rGO may provide more exposed catalytic active sites and a higher rate of mass transfer, which has been proven in carbon supports catalytic systems in previous reports [54,63–65].

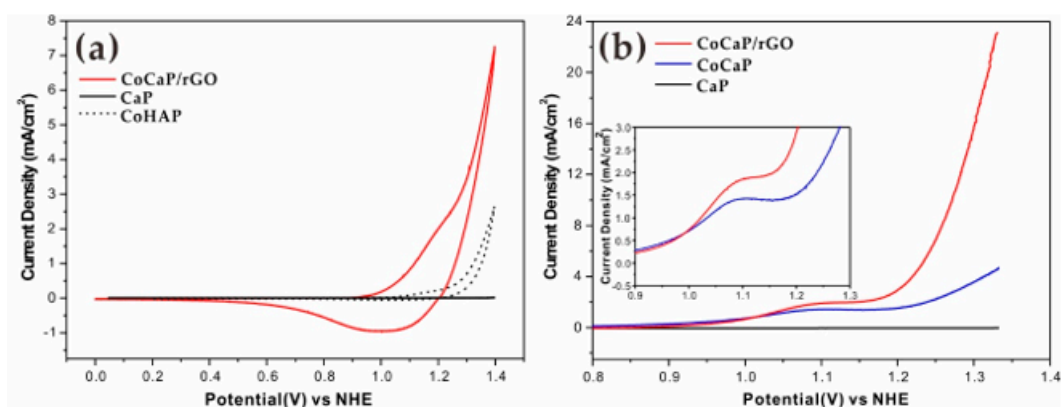


Figure 4. Cont.

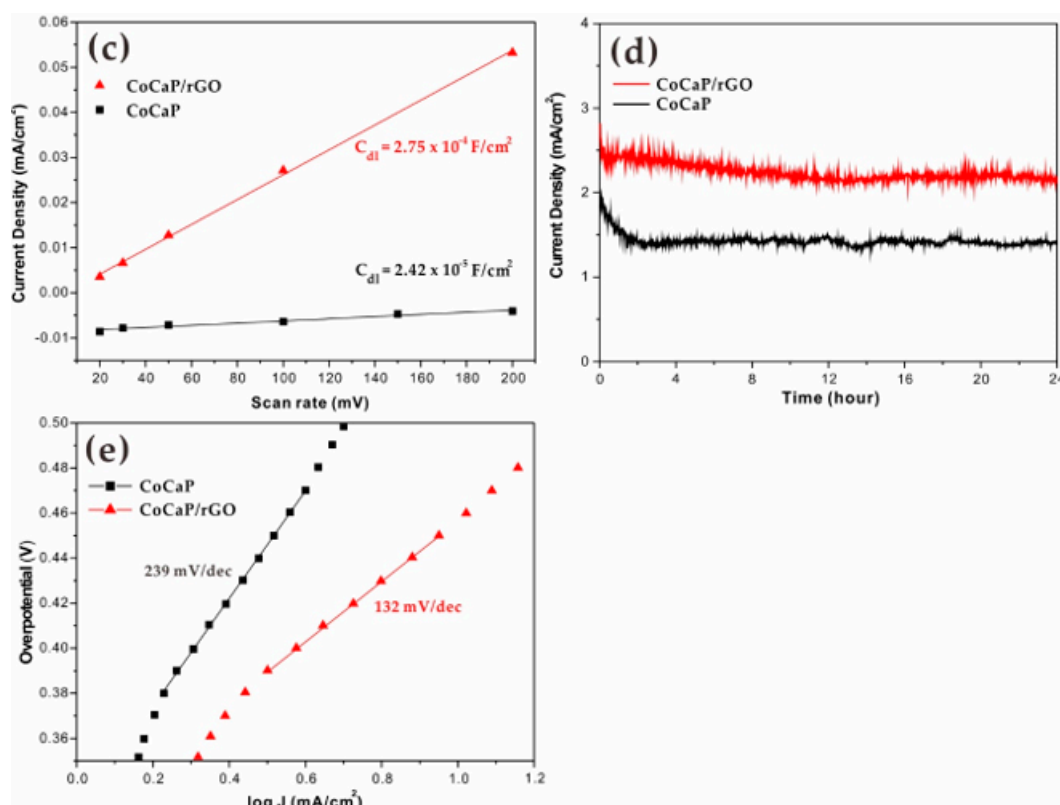


Figure 4. Electrochemical OER activities of CoCaP/rGO composites. (a) Cyclic voltammety in 0.1 M KPi buffer solution (pH 7), (b) LSV curves, (c) current density versus various scan rates, (d) bulk electrolysis of CoCaP/rGO on an ITO electrode at 1.5 V vs. NHE for 24 h in 0.1 M KPi buffer (pH 7) and (e) Tafel plots of CoCaP and CoCaP/rGO.

3. Materials and Methods

3.1. Materials

$\text{Ca}(\text{NO}_3)_2 \cdot 4\text{H}_2\text{O}$ (Duksan Chemicals, Ansan, Korea), Na_2HPO_4 (99.0%, Samchun Chemicals, Seoul, Korea), $\text{Co}(\text{NO}_3)_2 \cdot 6\text{H}_2\text{O}$ (Daejung chemicals, Siheung, Korea), K_2HPO_4 (Sigma Aldrich, >98%, Saint. Louis, MO, USA), KH_2PO_4 (Sigma Aldrich, St. Louis, MO, USA) and Nafion 117 containing solution (Sigma Aldrich, ~5 wt% in a mixture of lower aliphatic alcohols and water, Saint. Louis, MO, USA) are purchased and used without purification.

3.2. Preparation of Reduced Graphene Oxide (rGO)

The slightly modified Hummer's method was used to prepare graphene oxide (GO) [66]. 750 mg of graphite flakes were mixed with a 9:1 mixture of $\text{H}_2\text{SO}_4/\text{H}_3\text{PO}_4$ (90:10 mL) and stirred in an ice bath. Then, 4.5 g of potassium permanganate was added very slowly to the reaction mixture by maintaining the temperature at 35–40 °C. The reaction mixture was stirred at 50–55 °C for 12 h and then cooled to room temperature, followed by the addition of 100 mL of iced water containing 30% H_2O_2 [67–69]. The resulting solution was centrifuged at 8000 rpm for 30 min and the supernatant was removed. The gel-like product was washed 5–6 times with 50 mL of distilled water. GO powder was obtained by dialysis with the membrane for 3 days to remove acid in the product completely, followed by lyophilization for 3 days. A total of 250 mg of as-obtained GO powder were dispersed in 250 mL of DI water; then, the pH of the solution was adjusted to 10.0–11.0 by adding a trace amount of ammonium hydroxide solution (28%, *w/w*). A total of 1.25 mL of hydrazine hydrate were added to the solution and stirred at 95 °C for 1 h. The solution color became slightly darker as the reaction progressed [67–69]. The reaction mixture was centrifuged at 12,000 rpm for 30 min, then washed with DI water. Finally, the rGO dispersion was lyophilized to obtain rGO powder.

3.3. Preparation of Catalyst

Calcium phosphate [70] reduced graphene oxide (CaP/rGO) composite was prepared by the precipitation method. 20 mg of rGO powder were dispersed in 10 mL of DI water by ultrasonication for 1 h. 750 μ L of calcium nitrate tetrahydrate (0.656 M) were added into 10 mL of the rGO suspension, followed by addition of 750 μ L of sodium phosphate dibasic (0.394 M) solution. The reaction mixture was aged at 75 °C for 24 h. Finally, the CaP/rGO composite was obtained by washing using DI water for three times with centrifugation. The composite was lyophilized for 24 h. CaP was obtained by the same steps as preparing CoCaP/rGO without adding any rGO powder in the first step.

3.4. Preparation of Working Electrode

The glassy carbon electrode (5 mm in diameter) was cleaned with polishing using 1 μ m and 0.05 μ m alumina, followed by the sonication 3 \times 30 s in DI water. The Indium Tin Oxide (ITO) electrode was cleaned by the sonication 3 \times 30 s in DI water and acetone for two times, respectively. A total of 5 mg of as-obtained CaP/rGO composite were added into 150 μ L of ethanol and 80 μ L of 5% Nafion 117 solution [71]. This ink was ultrasonicated for 30 min. A total of 2.0 μ L and 10 μ L of ink were loaded onto glassy carbon electrode (0.197 cm²) and ITO electrode (area: 2 cm \times 0.5 cm) individually, then dried at ambient conditions.

3.5. In Situ Preparation of Cobalt Calcium Phosphate/rGO Composite (CoCaP/rGO)

The CoCaP/rGO was prepared by in situ anodic electrolysis. The electrolysis was done with a three-electrode electrochemical cell system using commercial potentiostat (EC Epsilon, BASi and ZIVE SP1, Wonatech). CaP/rGO on GCE (or ITO), Ag/AgCl and Pt-wire (or Pt plate) was used for a working, reference and counter electrode, respectively. The electrolysis was carried out under 50 mL of 20 mM cobalt nitrate solution by applying +1.3 V vs. NHE for 1 h without stirring. The CoCaP was prepared by the same way in the absence of rGO.

3.6. Characterization

The crystallinity of CoCaP/rGO film was determined by the X-ray diffraction (XRD, 3 kW Cu X-ray Diffractometer, D8 Advance, Bruker AXS, Hamburg, Germany). The shape of analysis of the CaP/rGO and CoCaP/rGO was performed using a Field Emission Transmission Electron Microscope (FE-TEM, JEM-F200, JEOL, Tokyo, Japan) and Scanning Electron Microscopy (SEM, JSM-6700F, JEOL, Tokyo, Japan). The morphology of the sample was analyzed using a holey carbon grid to map the carbon elements for TEM-EDS measurements. The surface elemental analysis was characterized by X-ray Photoelectron Spectroscopy (XPS, ULVAC-PHI Inc. PHI 5000 Versaprobe, Chigasaki, Japan). Electrochemical measurements were performed by a three-electrode electrochemical cell system with commercial potentiostats (EC Epsilon, BASi and ZIVE SP1, Wonatech). Linear sweep voltammetry (LSV) was carried out at 5 mV/s, and Tafel data were obtained from LSV. The electrochemical behavior of cyclic voltammetry was studied in 0.1 M potassium phosphate buffer solution (pH 7) with a sweep rate of 10 mV/s without iR compensation. Both CV and LSV were performed using a glassy carbon electrode (GCE) of 5 mm in diameter as the working electrode. The electrochemical double-layer capacitance (C_{dl}) was investigated using the CV method [72] in a potential range not affected by the faradaic current. All potentials were converted to the normal hydrogen electrode (NHE) using the following formula:

$$E(\text{NHE}) = E(\text{Ag}/\text{AgCl}) + 0.197 \text{ V} \quad (1)$$

The overpotential for oxygen evolution was calculated using the following formula:

$$\eta = E(\text{NHE}) + 0.059 \times \text{pH} - 1.23 \quad (2)$$

4. Conclusions

In summary, we prepared cobalt-calcium phosphate on reduced graphene oxide (CoCaP/rGO) by applying the anodic electrolysis in cobalt aqueous solution. During the anodic electrolysis process, the CaP/rGO was electrochemically converted into an amorphous phase of CoCaP/rGO and identified by XRD experiment. The TEM-EDS and XPS experiments of CoCaP/rGO suggest that amorphous cobalt oxide/phosphates are well dispersed on rGO. Furthermore, bulk electrolysis of chronoamperometric measurements demonstrated the stability of catalysts under the neutral conditions. Comparing the catalytic activity between CoCaP and CoCaP/rGO, we conclude that the dispersion of CoCaP on rGO with high conductivity enhanced catalytic activities in neutral conditions.

Supplementary Materials: The following are available online at <https://www.mdpi.com/article/10.3390/catal11080960/s1>: Figure S1: photographs taken in each step of the experiment; Figure S2: XRD patterns for CaHPO₄ (monetite), CaP/rGO and CoCaP/rGO and Miller facets of the nine peaks of CaHPO₄; Figure S3: TEM images and EDS elements mapping images of CaP/rGO; Figure S4: SEM images of CaP/rGO, CoCaP/rGO and EDS elemental mapping images of CoCaP/rGO; Figure S5: XPS spectrum comparing before and after anodic electrolysis of CaP/rGO; Figure S6: cyclic voltammetry experiments of the current density of CoCaP and CoCaP/rGO composite; Video S1: the anodic electrolysis of CaP/rGO for 1 h in 20 mM Co²⁺ aqueous solution; Video S2: the surface of CoCaP/rGO-coated ITO electrode at 1.5 V vs. NHE in 0.1 M KPi (pH 7); Table S1: the crystal size of CaHPO₄ derived from XRD peaks using the Scherrer equation.

Author Contributions: K.-Y.K. and D.-K.L. conceived and designed the experiments; K.L. performed the syntheses of catalysts and the examination of catalytic properties; E.P., H.C. and Y.C. contributed to the scientific discussion; S.L. and C.S.K. contributed XRD and XPS experiments; W.Y. synthesized the reduced graphene oxide and contributed TEM-EDS experiments; K.-Y.K. and K.L. wrote the manuscript. All authors have read and agreed to the published version of the manuscript.

Funding: This work was supported by the Basic Science Research Program through the National Research Foundation of Korea (NRF), funded by the Ministry of Education (NRF-2019R111A3A0105983712, K.-Y.K.) and National Research Fund of Korea (2018R1A2A3075499, D.-K.L.).

Data Availability Statement: The data are contained within the article.

Conflicts of Interest: The authors declare no conflict of interest.

References

1. Lewis, N.S.; Nocera, D.G. Powering the planet: Chemical challenges in solar energy utilization. *Proc. Natl. Acad. Sci. USA* **2006**, *103*, 15729–15735. [[CrossRef](#)] [[PubMed](#)]
2. Kiwi, J.; Grätzel, M. Oxygen Evolution from Water via Redox Catalysis. *Angew. Chem. Int. Ed.* **1978**, *17*, 860–861. [[CrossRef](#)]
3. Galizzioli, D.; Tantardini, F.; Trasatti, S. Ruthenium dioxide: A new electrode material. I. Behaviour in acid solutions of inert electrolytes. *J. Appl. Electrochem.* **1974**, *4*, 57–67. [[CrossRef](#)]
4. Lee, Y.; Suntivich, J.; May, K.J.; Perry, E.E.; Shao-Horn, Y. Synthesis and activities of rutile IrO₂ and RuO₂ nanoparticles for oxygen evolution in acid and alkaline solutions. *J. Phys. Chem. Lett.* **2012**, *3*, 399–404. [[CrossRef](#)] [[PubMed](#)]
5. Reier, T.; Oezaslan, M.; Strasser, P. Electrocatalytic oxygen evolution reaction (OER) on Ru, Ir, and Pt catalysts: A comparative study of nanoparticles and bulk materials. *ACS Catal.* **2012**, *2*, 1765–1772. [[CrossRef](#)]
6. Cherevko, S.; Geiger, S.; Kasian, O.; Kulyk, N.; Grote, J.P.; Savan, A.; Shrestha, B.R.; Merzlikin, S.; Breitbach, B.; Ludwig, A.; et al. Oxygen and hydrogen evolution reactions on Ru, RuO₂, Ir, and IrO₂ thin film electrodes in acidic and alkaline electrolytes: A comparative study on activity and stability. *Catal. Today* **2016**, *262*, 170–180. [[CrossRef](#)]
7. Gray, H.B. Powering the planet with solar fuel. *Nat. Chem.* **2009**, *1*, 7. [[CrossRef](#)]
8. Yang, Y.; Fei, H.; Ruan, G.; Tour, J.M. Porous cobalt-based thin film as a bifunctional catalyst for hydrogen generation and oxygen generation. *Adv. Mater.* **2015**, *27*, 3175–3180. [[CrossRef](#)]
9. Jin, H.; Wang, J.; Su, D.; Wei, Z.; Pang, Z.; Wang, Y. In Situ Cobalt–Cobalt Oxide/N-Doped Carbon Hybrids as Superior Bifunctional Electrocatalysts for Hydrogen and Oxygen Evolution. *J. Am. Chem. Soc.* **2015**, *137*, 2688–2694. [[CrossRef](#)]
10. Dou, S.; Tao, L.; Huo, J.; Wang, S.; Dai, L. Etched and doped Co₉S₈/graphene hybrid for oxygen electrocatalysis. *Energy Environ. Sci.* **2016**, *9*, 1320–1326. [[CrossRef](#)]
11. Qiao, X.; Jin, J.; Fan, H.; Cui, L.; Ji, S.; Li, Y.; Liao, S. Cobalt and Nitrogen Co-Doped Graphene–Carbon Nanotube Aerogel as an Efficient Bifunctional Electrocatalyst for Oxygen Reduction and Evolution Reactions. *Catalysts* **2018**, *8*, 275. [[CrossRef](#)]

12. Ahsan, M.A.; Puente Santiago, A.R.; Hong, Y.; Zhang, N.; Cano, M.; Rodriguez-Castellon, E.; Echegoyen, L.; Sreenivasan, S.T.; Noveron, J.C. Tuning of Trifunctional NiCu Bimetallic Nanoparticles Confined in a Porous Carbon Network with Surface Composition and Local Structural Distortions for the Electrocatalytic Oxygen Reduction, Oxygen and Hydrogen Evolution Reactions. *J. Am. Chem. Soc.* **2020**, *142*, 14688–14701. [[CrossRef](#)] [[PubMed](#)]
13. Li, J.S.; Li, S.L.; Tang, Y.J.; Han, M.; Dai, Z.H.; Bao, J.C.; Lan, Y.Q. Nitrogen-doped Fe/Fe₃C@graphitic layer/carbon nanotube hybrids derived from MOFs: Efficient bifunctional electrocatalysts for ORR and OER. *Chem. Commun.* **2015**, *51*, 2710–2713. [[CrossRef](#)] [[PubMed](#)]
14. Wang, Q.; Lei, Y.; Chen, Z.; Wu, N.; Wang, Y.; Wang, B.; Wang, Y. Fe/Fe₃C@C nanoparticles encapsulated in N-doped graphene-CNTs framework as an efficient bifunctional oxygen electrocatalyst for robust rechargeable Zn-air batteries. *J. Mater. Chem. A* **2018**, *6*, 516–526. [[CrossRef](#)]
15. Jia, Y.; Zhang, L.; Gao, G.; Chen, H.; Wang, B.; Zhou, J.; Soo, M.T.; Hong, M.; Yan, X.; Qian, G.; et al. A Heterostructure Coupling of Exfoliated Ni-Fe Hydroxide Nanosheet and Defective Graphene as a Bifunctional Electrocatalyst for Overall Water Splitting. *Adv. Mater.* **2017**, *29*, 1700017. [[CrossRef](#)]
16. Yu, X.; Zhang, M.; Yuan, W.; Shi, G. A high-performance three-dimensional Ni-Fe layered double hydroxide/graphene electrode for water oxidation. *J. Mater. Chem. A* **2015**, *3*, 6921–6928. [[CrossRef](#)]
17. Bao, J.; Xie, J.; Lei, F.; Wang, Z.; Liu, W.; Xu, L.; Guan, M.; Zhao, Y.; Li, H. Two-Dimensional Mn-Co LDH/Graphene Composite towards High-Performance Water Splitting. *Catalysts* **2018**, *8*, 350. [[CrossRef](#)]
18. Liu, Y.; Jiang, H.; Zhu, Y.; Yang, X.; Li, C. Transition metals (Fe, Co, and Ni) encapsulated in nitrogen-doped carbon nanotubes as bi-functional catalysts for oxygen electrode reactions. *J. Mater. Chem. A* **2016**, *4*, 1694–1701. [[CrossRef](#)]
19. Yan, W.; Bian, W.; Jin, C.; Tian, J.-H.; Yang, R. An Efficient Bi-functional Electrocatalyst Based on Strongly Coupled CoFe₂O₄/Carbon Nanotubes Hybrid for Oxygen Reduction and Oxygen Evolution. *Electrochim. Acta* **2015**, *177*, 65–72. [[CrossRef](#)]
20. Zhang, X.; Xu, H.; Li, X.; Li, Y.; Yang, T.; Liang, Y. Facile Synthesis of Nickel-Iron/Nanocarbon Hybrids as Advanced Electrocatalysts for Efficient Water Splitting. *ACS Catal.* **2016**, *6*, 580–588. [[CrossRef](#)]
21. Mao, S.; Pu, H.; Chen, J. Graphene oxide and its reduction: Modeling and experimental progress. *RSC Adv.* **2012**, *2*, 2643–2662. [[CrossRef](#)]
22. Dreyer, D.R.; Park, S.; Bielawski, C.W.; Ruoff, R.S. The chemistry of graphene oxide. *Chem. Soc. Rev.* **2010**, *39*, 228–240. [[CrossRef](#)]
23. Zhu, Y.; Murali, S.; Cai, W.; Li, X.; Suk, J.W.; Potts, J.R.; Ruoff, R.S. Graphene and graphene oxide: Synthesis, properties, and applications. *Adv. Mater.* **2010**, *22*, 3906–3924. [[CrossRef](#)] [[PubMed](#)]
24. Park, S.; Ruoff, R.S. Chemical methods for the production of graphenes. *Nat. Nanotechnol.* **2009**, *4*, 217–224. [[CrossRef](#)]
25. Liang, Y.; Li, Y.; Wang, H.; Zhou, J.; Wang, J.; Regier, T.; Dai, H. Co₃O₄ nanocrystals on graphene as a synergistic catalyst for oxygen reduction reaction. *Nat. Mater.* **2011**, *10*, 780–786. [[CrossRef](#)]
26. Mao, S.; Wen, Z.; Huang, T.; Hou, Y.; Chen, J. High-performance bi-functional electrocatalysts of 3D crumpled graphene-cobalt oxide nanohybrids for oxygen reduction and evolution reactions. *Energy Environ. Sci.* **2014**, *7*, 609–616. [[CrossRef](#)]
27. Long, X.; Li, J.; Xiao, S.; Yan, K.; Wang, Z.; Chen, H.; Yang, S. A strongly coupled graphene and FeNi double hydroxide hybrid as an excellent electrocatalyst for the oxygen evolution reaction. *Angew. Chem. Int. Ed.* **2014**, *53*, 7584–7588. [[CrossRef](#)]
28. Liu, Q.; Jin, J.; Zhang, J. NiCo₂S₄@graphene as a bifunctional electrocatalyst for oxygen reduction and evolution reactions. *ACS Appl. Mater. Interfaces* **2013**, *5*, 5002–5008. [[CrossRef](#)]
29. Jahan, M.; Liu, Z.; Loh, K.P. A graphene oxide and copper-centered metal organic framework composite as a tri-functional catalyst for HER, OER, and ORR. *Adv. Funct. Mater.* **2013**, *23*, 5363–5372. [[CrossRef](#)]
30. Kanan, M.W.; Nocera, D.G. In situ formation of an oxygen-evolving catalyst in neutral water containing phosphate and Co²⁺. *Science* **2008**, *321*, 1072–1075. [[CrossRef](#)] [[PubMed](#)]
31. Surendranath, Y.; Kanan, M.W.; Nocera, D.G. Mechanistic studies of the oxygen evolution reaction by a cobalt-phosphate catalyst at neutral pH. *J. Am. Chem. Soc.* **2010**, *132*, 16501–16509. [[CrossRef](#)]
32. Esswein, A.J.; Surendranath, Y.; Reece, S.Y.; Nocera, D.G. Highly active cobalt phosphate and borate based oxygen evolving catalysts operating in neutral and natural waters. *Energy Environ. Sci.* **2011**, *4*, 499–504. [[CrossRef](#)]
33. Kanan, M.W.; Yano, J.; Surendranath, Y.; Dincă, M.; Yachandra, V.K.; Nocera, D.G. Structure and valency of a cobalt-phosphate water oxidation catalyst determined by in situ X-ray spectroscopy. *J. Am. Chem. Soc.* **2010**, *132*, 13692–13701. [[CrossRef](#)]
34. Kanan, M.W.; Surendranath, Y.; Nocera, D.G. Cobalt-phosphate oxygen-evolving compound. *Chem. Soc. Rev.* **2009**, *38*, 109–114. [[CrossRef](#)]
35. Surendranath, Y.; Dincă, M.; Nocera, D.G. Electrolyte-Dependent Electrosynthesis and Activity of Cobalt-Based Water Oxidation Catalysts. *J. Am. Chem. Soc.* **2009**, *131*, 2615–2620. [[CrossRef](#)] [[PubMed](#)]
36. Brodsky, C.N.; Bediako, D.K.; Shi, C.; Keane, T.P.; Costentin, C.; Billinge, S.J.L.; Nocera, D.G. Proton-Electron Conductivity in Thin Films of a Cobalt-Oxygen Evolving Catalyst. *ACS Appl. Energy Mater.* **2019**, *2*, 3–12. [[CrossRef](#)]
37. Xie, L.; Zhang, R.; Cui, L.; Liu, D.; Hao, S.; Ma, Y.; Du, G.; Asiri, A.M.; Sun, X. High-Performance Electrolytic Oxygen Evolution in Neutral Media Catalyzed by a Cobalt Phosphate Nanoarray. *Angew. Chem. Int. Ed.* **2017**, *56*, 1064–1068. [[CrossRef](#)]
38. Pyo, E.; Lee, K.; Jang, M.J.; Ko, I.H.; Kim, C.S.; Choi, S.M.; Lee, S.; Kwon, K.Y. Cobalt Incorporated Hydroxyapatite Catalyst for Water Oxidation. *ChemCatChem* **2019**, *11*, 5425–5429. [[CrossRef](#)]
39. Jaworski, J.W.; Cho, S.; Kim, Y.; Jung, J.H.; Jeon, H.S.; Min, B.K.; Kwon, K.Y. Hydroxyapatite supported cobalt catalysts for hydrogen generation. *J. Colloid Interface Sci.* **2013**, *394*, 401–408. [[CrossRef](#)]

40. Han, A.; Wu, H.; Sun, Z.; Jia, H.; Yan, Z.; Ma, H.; Liu, X.; Du, P. Green Cobalt Oxide (CoO_x) Film with Nanoribbon Structures Electrodeposited from the BF₂-Annulated Cobaloxime Precursor for Efficient Water Oxidation. *ACS Appl. Mater. Interfaces* **2014**, *6*, 10929–10934. [[CrossRef](#)] [[PubMed](#)]
41. Tian, J.; Li, H.; Asiri, A.M.; Al-Youbi, A.O.; Sun, X. Photoassisted Preparation of Cobalt Phosphate/Graphene Oxide Composites: A Novel Oxygen-Evolving Catalyst with High Efficiency. *Small* **2013**, *9*, 2709–2714. [[CrossRef](#)]
42. Han, A.; Wu, H.; Sun, Z.; Jia, H.; Du, P. Facile deposition of nanostructured cobalt oxide catalysts from molecular cobaloximes for efficient water oxidation. *Phys. Chem. Chem. Phys.* **2013**, *15*, 12534–12538. [[CrossRef](#)] [[PubMed](#)]
43. González-Flores, D.; Sánchez, I.; Zaharieva, I.; Klingan, K.; Heidkamp, J.; Chernev, P.; Menezes, P.W.; Driess, M.; Dau, H.; Montero, M.L. Heterogeneous Water Oxidation: Surface Activity versus Amorphization Activation in Cobalt Phosphate Catalysts. *Angew. Chem. Int. Ed.* **2015**, *54*, 2472–2476. [[CrossRef](#)]
44. Menezes, P.W.; Panda, C.; Walter, C.; Schwarze, M.; Driess, M. A Cobalt-Based Amorphous Bifunctional Electrocatalysts for Water-Splitting Evolved from a Single-Source Lazulite Cobalt Phosphate. *Adv. Funct. Mater.* **2019**, *29*, 1808632. [[CrossRef](#)]
45. Kim, D.; Lee, S.; Woo, D.; Byun, J.; Kwon, K. Synthesis and Morphological Characterization of Calcium Phosphates Prepared under Different NaOH Concentrations. *Bull. Korean Chem. Soc.* **2014**, *35*, 2241–2242. [[CrossRef](#)]
46. Liu, Y.; Nocera, D.G. Spectroscopic Studies of Nanoparticulate Thin Films of a Cobalt-Based Oxygen Evolution Catalyst. *J. Phys. Chem. C* **2014**, *118*, 17060–17066. [[CrossRef](#)]
47. Ryu, J.; Jung, N.; Jang, J.H.; Kim, H.-J.; Yoo, S.J. In Situ Transformation of Hydrogen-Evolving CoP Nanoparticles: Toward Efficient Oxygen Evolution Catalysts Bearing Dispersed Morphologies with Co-oxo/hydroxo Molecular Units. *ACS Catal.* **2015**, *5*, 4066–4074. [[CrossRef](#)]
48. Chusuei, C.C.; Goodman, D.W.; Van Stipdonk, M.J.; Justes, D.R.; Schweikert, E.A. Calcium Phosphate Phase Identification Using XPS and Time-of-Flight Cluster SIMS. *Anal. Chem.* **1999**, *71*, 149–153. [[CrossRef](#)]
49. Lu, H.B.; Campbell, C.T.; Graham, D.J.; Ratner, B.D. Surface Characterization of Hydroxyapatite and Related Calcium Phosphates by XPS and TOF-SIMS. *Anal. Chem.* **2000**, *72*, 2886–2894. [[CrossRef](#)]
50. Ahn, H.S.; Tilley, T.D. Electrocatalytic Water Oxidation at Neutral pH by a Nanostructured Co(PO₃)₂ Anode. *Adv. Funct. Mater.* **2013**, *23*, 227–233. [[CrossRef](#)]
51. Burke, M.S.; Zou, S.; Enman, L.J.; Kellon, J.E.; Gabor, C.A.; Pledger, E.; Boettcher, S.W. Revised Oxygen Evolution Reaction Activity Trends for First-Row Transition-Metal (Oxy)hydroxides in Alkaline Media. *J. Phys. Chem. Lett.* **2015**, *6*, 3737–3742. [[CrossRef](#)]
52. Han, B.; Qian, D.; Risch, M.; Chen, H.; Chi, M.; Meng, Y.S.; Shao-Horn, Y. Role of LiCoO₂ Surface Terminations in Oxygen Reduction and Evolution Kinetics. *J. Phys. Chem. Lett.* **2015**, *6*, 1357–1362. [[CrossRef](#)]
53. Yang, L.; Lv, Y.; Cao, D. Co,N-codoped nanotube/graphene 1D/2D heterostructure for efficient oxygen reduction and hydrogen evolution reactions. *J. Mater. Chem. A* **2018**, *6*, 3926–3932. [[CrossRef](#)]
54. Liu, X.; Liu, W.; Ko, M.; Park, M.; Kim, M.G.; Oh, P.; Chae, S.; Park, S.; Casimir, A.; Wu, G.; et al. Metal (Ni, Co)-Metal Oxides/Graphene Nanocomposites as Multifunctional Electrocatalysts. *Adv. Funct. Mater.* **2015**, *25*, 5799–5808. [[CrossRef](#)]
55. Li, Y.; Wang, H.; Xie, L.; Liang, Y.; Hong, G.; Dai, H. MoS₂ Nanoparticles Grown on Graphene: An Advanced Catalyst for the Hydrogen Evolution Reaction. *J. Am. Chem. Soc.* **2011**, *133*, 7296–7299. [[CrossRef](#)]
56. Ge, R.; Du, H.; Tao, K.; Zhang, Q.; Chen, L. Cobalt-Borate Nanoarray: An Efficient and Durable Electrocatalyst for Water Oxidation under Benign Conditions. *ACS Appl. Mater. Interfaces* **2017**, *9*, 15383–15387. [[CrossRef](#)]
57. Aksoy, M.; Nune, S.V.K.; Karadas, F. A Novel Synthetic Route for the Preparation of an Amorphous Co/Fe Prussian Blue Coordination Compound with High Electrocatalytic Water Oxidation Activity. *Inorg. Chem.* **2016**, *55*, 4301–4307. [[CrossRef](#)]
58. Pintado, S.; Goberna-Ferrón, S.; Escudero-Adán, E.C.; Galán-Mascarós, J.R. Fast and Persistent Electrocatalytic Water Oxidation by Co-Fe Prussian Blue Coordination Polymers. *J. Am. Chem. Soc.* **2013**, *135*, 13270–13273. [[CrossRef](#)] [[PubMed](#)]
59. Li, K.; Zhang, J.; Wu, R.; Yu, Y.; Zhang, B. Anchoring CoO Domains on CoSe₂ Nanobelts as Bifunctional Electrocatalysts for Overall Water Splitting in Neutral Media. *Adv. Sci.* **2016**, *3*, 1500426. [[CrossRef](#)]
60. Chen, S.; Duan, J.; Jaroniec, M.; Qiao, S.Z. Three-Dimensional N-Doped Graphene Hydrogel/NiCo Double Hydroxide Electrocatalysts for Highly Efficient Oxygen Evolution. *Angew. Chem. Int. Ed.* **2013**, *52*, 13567–13570. [[CrossRef](#)]
61. Bian, W.; Yang, Z.; Strasser, P.; Yang, R. A CoFe₂O₄/graphene nanohybrid as an efficient bi-functional electrocatalyst for oxygen reduction and oxygen evolution. *J. Power Sources* **2014**, *250*, 196–203. [[CrossRef](#)]
62. Zhao, Y.; Chen, S.; Sun, B.; Su, D.; Huang, X.; Liu, H.; Yan, Y.; Sun, K.; Wang, G. Graphene-Co₃O₄ nanocomposite as electrocatalyst with high performance for oxygen evolution reaction. *Sci. Rep.* **2015**, *5*, 7629. [[CrossRef](#)] [[PubMed](#)]
63. Chen, P.; Xu, K.; Zhou, T.; Tong, Y.; Wu, J.; Cheng, H.; Lu, X.; Ding, H.; Wu, C.; Xie, Y. Strong-Coupled Cobalt Borate Nanosheets/Graphene Hybrid as Electrocatalyst for Water Oxidation Under Both Alkaline and Neutral Conditions. *Angew. Chem. Int. Ed.* **2016**, *55*, 2488–2492. [[CrossRef](#)] [[PubMed](#)]
64. Li, Y.; Zhao, Y.; Zhang, Z. A porous graphene/cobalt phosphate composite as an efficient oxygen evolving catalyst. *Electrochem. Commun.* **2014**, *48*, 35–39. [[CrossRef](#)]
65. Mao, S.; Wen, Z.; Kim, H.; Lu, G.; Hurley, P.; Chen, J. A General Approach to One-Pot Fabrication of Crumpled Graphene-Based Nanohybrids for Energy Applications. *ACS Nano* **2012**, *6*, 7505–7513. [[CrossRef](#)] [[PubMed](#)]
66. Li, D.; Müller, M.B.; Gilje, S.; Kaner, R.B.; Wallace, G.G. Processable aqueous dispersions of graphene nanosheets. *Nat. Nanotechnol.* **2008**, *3*, 101–105. [[CrossRef](#)] [[PubMed](#)]

67. Lim, D.-K.; Barhoumi, A.; Wylie, R.G.; Reznor, G.; Langer, R.S.; Kohane, D.S. Enhanced Photothermal Effect of Plasmonic Nanoparticles Coated with Reduced Graphene Oxide. *Nano Lett.* **2013**, *13*, 4075–4079. [[CrossRef](#)] [[PubMed](#)]
68. Moon, H.; Kumar, D.; Kim, H.; Sim, C.; Chang, J.-H.; Kim, J.-M.; Kim, H.; Lim, D.-K. Amplified Photoacoustic Performance and Enhanced Photothermal Stability of Reduced Graphene Oxide Coated Gold Nanorods for Sensitive Photoacoustic Imaging. *ACS Nano* **2015**, *9*, 2711–2719. [[CrossRef](#)]
69. Kumar, D.; Lee, A.; Lee, T.; Lim, M.; Lim, D.-K. Ultrafast and Efficient Transport of Hot Plasmonic Electrons by Graphene for Pt Free, Highly Efficient Visible-Light Responsive Photocatalyst. *Nano Lett.* **2016**, *16*, 1760–1767. [[CrossRef](#)] [[PubMed](#)]
70. Tamimi, F.; Sheikh, Z.; Barralet, J. Dicalcium phosphate cements: Brushite and monetite. *Acta Biomater.* **2012**, *8*, 474–487. [[CrossRef](#)]
71. Fuller, T.F.; Newman, J. Experimental Determination of the Transport Number of Water in Nafion 117 Membrane. *J. Electrochem. Soc.* **1992**, *139*, 1332–1337. [[CrossRef](#)]
72. Anantharaj, S.; Ede, S.R.; Karthick, K.; Sam Sankar, S.; Sangeetha, K.; Karthik, P.E.; Kundu, S. Precision and correctness in the evaluation of electrocatalytic water splitting: Revisiting activity parameters with a critical assessment. *Energy Environ. Sci.* **2018**, *11*, 744–771. [[CrossRef](#)]